Cite This: ACS Sustainable Chem. Eng. XXXX, XXX, XXX-XXX

Effect of Reaction Time on Phosphate Mineralization from Microalgae Hydrolysate

Ali Teymouri, Ben J. Stuart, and Sandeep Kumar*

Department of Civil & Environmental Engineering, Old Dominion University, Norfolk, Virginia 23529, United States

Supporting Information

ABSTRACT: The development of algal biorefineries is strongly associated with the nutrient management, particularly phosphorus, which is a limited mineral resource. Flash hydrolysis (FH) has been widely applied to a variety of algae species to fractionate its constituents. This chemical-free, subcritical water technique was used to extract more than 80 wt % of phosphorus available in the Scenedesmus sp. as watersoluble phosphates in the aqueous phase (hydrolysate). The phosphate-rich hydrolysate was subjected to the hydrothermal mineralization (HTM) process at 280 °C and 5-90 min of



residence time to mineralize phosphates as allotropes of calcium phosphate such as hydroxyapatite (HAp) and whitlockite (WH). In the current study, the effect of reaction time on phosphate mineralization from the hydrolysate as well as the composition, structure and the morphology of the precipitates were studied. Calcium hydroxide and commercial HAp were used as the mineralizer and seeding material, respectively. More than 97 wt % of phosphate and almost 94 wt % of calcium were removed in the first 5 min of the HTM process. Results revealed that as the HTM reaction time increased, calcium phosphate precipitates transformed from WH to carbonated HAp. The integration of the proposed mineralization process with FH can be a costeffective pathway to produce sustainable, and high value phosphate-based bioproducts from algae. The application of HAp includes biomedical applications such as synthetic bone and implant filling, drug delivery, chromatography, corrosion resistance materials, catalytic activities and fertilizers.

KEYWORDS: Microalgae, Flash hydrolysis, Hydrothermal mineralization, Nutrients removal, Phosphorus, Hydroxyapatite, Whitlockite

INTRODUCTION

The US Department of Energy (DOE) has set up a target production of 60 billion gallons per year (BGY) of biofuels, which is equal to 30% of the US transportation fuels by 2030. Microalgae is a promising feedstock for the biofuels and bioproducts production. Numerous studies have been conducted to commercialize the process; however, due to a number of technical challenges such as microalgae species selection, large-scale productivity potential, resource availability, cultivation, harvesting, and chosen oil extraction technique, the development is far behind in industrial production. ^{1,2} Technoeconomic analysis (TEA) and life cycle assessment (LCA) have pointed out considerable amount of costs associated with the nutrient (N & P) supply and recommends the production of value-added bioproducts to enhance the sustainability and costeffectiveness of the overall process.³ In addition to cost, availability of nutrients, particularly phosphorus, which is derived from an irreplaceable resource, has always been a major concern. A recent study by Shurtz et al. highlighted the 3.85 and 0.87 million metric tons (Mmt) of nitrogen and phosphorus requirement respectively, for the 10 BGY of renewable fuel production.³ This amount is significant comparing to the total 7.71 Mmt phosphate (P_2O_5) rock production in the US in 2015.4 This will substantially affect the

fertilizer market which may result in food cost increase. Furthermore, from the bioenergy point of view, phosphorus is toxic for automotive exhaust catalyst.⁵ Therefore, seeking a comprehensive method that could recover phosphorus content of microalgae in form of byproducts could facilitate the algal processing industry.

Flash hydrolysis (FH) has been widely applied as an environmentally benign process that capitalizes on the difference in reaction kinetics of algae components to extract nutrients in the aqueous phase (hydrolysate), while retaining the lipids in the solid phase known as biofuels intermediates. A variety of microalgae feedstocks have been tested through FH technique to extract nutrients.⁶⁻¹² It has been shown that 280 °C and 10 s of residence time is the optimum condition regarding nutrients extraction efficiency.⁸ Applying this technique to Scenedesmus sp. slurry resulted in more than 80 wt % of phosphorus and 60 wt % of nitrogen present in the hydrolysate fraction. Our prior studies^{9,10} have demonstrated the feasibility of hydrolysate for direct nutrients recycling, which is suitable for a scenario where storage of algae

Received: August 24, 2017 Revised: November 9, 2017 Published: November 14, 2017 hydrolysate is neither required nor available. However, direct recycling of nutrients is not a viable option whenever storage of nutrients (algae hydrolysate) for algae cultivation is envisioned. The organic compounds in the hydrolysate favors bacterial growth and makes it a nonviable option for the storage of this dilute aqueous stream. An alternative option is to develop a process that can convert these nutrients to nonperishable high value bioproducts.

Hydrothermal mineralization (HTM) is a technique that has been conceptually driven from the earth-mimetic deposit phenomena and has been used to precipitate ions out of the aqueous phase. The method has been already applied for detoxification of water as well as resource recovery. 13,14 Our previous study focused on integration of the FH and HTM or FH and AP (atmospheric precipitation) processes in order to recover phosphorus from algae hydrolysate in the form of products such as hydroxyapatite (HAp, Ca₁₀(PO₄)₆(OH)₂) and/or whitlockite (WH, Ca₁₈Mg₂(HPO₄)₂(PO₄)₁₂), and dittmarite (magnesium ammonium phosphate, MAP, MgNH₄PO₄·H₂O). This study provided a basis for further experimental studies to understand the mechanism of HAp formation and the effect of time on phosphate mineralization.

HAp is the most stable calcium orthophosphate at pH above 4 and has a variety of chemical and biomedical applications, including bone tissue regeneration, cell proliferation, drug delivery, implant coating, and catalytic activity. 15-17 HAp has been produced through methods such as chemical precipitation, electrospinning, electrospraying, solid state, microwave irradiation, self-propagating combustion, emulsion and microemulsion, surfactant assisted precipitation, chemical vapor, flux cooling, and hydrothermal processing. 18 Among these options, hydrothermal method is favored, due to the ability of producing a pure phase with high crystallinity. 19 The hydrothermal studies for HAp production used a long reaction time (few hours to days), while using pure calcium and phosphorus containing compounds as reactants. ^{20,21} It is also theorized that HAp synthesis for biomedical application from natural reactants, such as microalgae hydrolysate has higher chance to get accepted by an organism in human body.²² On the other hand, WH is known as the second component in hard tissue after HAp.²³ Although studies on WH showed better bone regeneration compared to HAp, 24 its synthetic mechanism and role in the body has not yet been well understood.²⁵

Our prior study has confirmed the recovery of almost 83 wt % of phosphorus from microalgae in the form of carbonate HAp and WH via the integrated FH-HTM process at 280 °C and 1 h of residence time. In the same study, ²⁶ we identified the significant role of seeding materials to promote crystallization in the precipitation process. To date, no study was carried out about the kinetics of HAp and WH under hydrothermal condition. However, few studies investigated HAp as well as WH formation through precipitation process at temperatures below 90 °C. Tomson and Nancollas suggested that octacalcium phosphate is the precursor to HAp precipitation at physiological pH.²⁷ This idea was then supported by Liu et al. on the precipitation of HAp at pH between 10 and 11. They introduced following steps for HAp synthesis: transferring from octacalcium phosphate (OCP) to amorphous calcium phosphate (ACP) and then to calcium-deficient hydroxyapatite and HAp.²⁸ Furthermore, it has been noted that HAp formation kinetics are initially controlled by surface areas of the reactants, whereas the rate of formation is controlled by diffusion.²⁹ On the other hand, pure WH nanoparticles (without any

intermediate phases) were precipitated in a ternary Ca-(OH)₂-Mg(OH)₂-H₃PO₄ system under acidic condition (pH < 4.2) with excess Mg^{2+} to impede the HAp growth.²³ Their study revealed that in the presence of Mg²⁺, after reducing pH, HAp transformed into dicalcium phosphate dehydrate and then into WH. Although, none of the above studies are in hydrothermal conditions, they will still guide us through the possible HAp and WH production mechanisms.

The current study investigates the effect of HTM reaction time on the phosphate mineralization process and the chemistry of calcium phosphate precipitates. To this aim, we seek the following objectives: (1) evaluating phosphate and calcium removal from the aqueous phase after each HTM experiment, (2) characterizing liquid and solid phases associated with every stage of this study as well as the initial algal biomass, (3) assessing the composition, structure, thermal stability, crystallinity, and morphology of minerals precipitated at different reaction times. This is the first kind of study in which the kinetics of calcium phosphate precipitates from algae hydrolysate is being investigated. Understanding the kinetics of phosphate removal and the bioproducts formation pathways from the algae hydrolysate will lead to a smarter energy and material integration, resource utilization, as well as an efficient, reliable, and economic design of downstream processes in the algal biorefineries.

MATERIALS AND METHODS

Microalgae Characterization. Scenedesmus sp. was cultivated in the Biomass Research Laboratory (BRL) at Old Dominion University using the BG-11 media as explained in our previous study. Following harvesting, microalgae were freeze-dried and stored in plastic airtight bottles at below -20 °C until the experiment. Microalgae were fully characterized by performing proximate and ultimate analysis using thermogravimetric analysis (TGA) (TGA-50H, Shimadzu Corporation) and Thermo Finnigan Flash EA 1112 automatic elemental analyzer (ThermoFisher Scientific, Waltham, MA), respectively. For ultimate analysis, 2,5-Bis(5-tert-butyl-benzoxazol-2-yl) thiophene (BBOT) standard (certified# 202147-10/03/2015, ThermoFisher Scientific, Cambridge, UK) were used as a standard. The EA combustion furnace was set at 950 °C while the oven was at 65 °C. Helium was used as a carrier gas with the flow of 100 mL/min. All experiments were conducted in triplicate and the reported values are the averages. Moisture and volatile analysis were calculated through a pyrolysis process using nitrogen flow. The temperature was ramped (10 °C/min) to 90 °C, then, was increased in a stepwise function (1 °C/min) to 110 °C. Again, the temperature was ramped (10 °C/min) to 800 °C and was increased in a stepwise function (1 °C/min) until 850 °C. Moisture and volatile content were then calculated based on zero weight losses at 100 and 850 °C, respectively. The sample was cooled down to 120 °C and after switching the flow to compressed air, ramped (10 °C/min) to 800 °C for the combustion process to calculate ash and fixed carbon. Finally, the sample entered the last stepwise function (1 °C/min) to 850 °C and held until the derivative weight change was less than 0.01 wt %/min.

Experimental Procedure. More than 10 FH experiments were performed at optimum conditions to collect enough hydrolysate for this study. Optimum conditions for maximum nutrient recovery, which were 280 °C and 10 s of residence time, was selected based on our previous studies.^{6,8} Following each run, products were subjected to solid liquid separation using Fisher Scientific accuSpinTM 400 centrifuge and vacuum filtration. Biofuels intermediates that preserved most of the lipids, were stored at below −20 °C. Hydrolysate were analyzed for total organic carbon (TOC) and total nitrogen (TN) using Shimadzu TOC/TN analyzer (TOC-V_{CSN}, Shimadzu) equipped with an ASI-V auto sampler to ensure its homogeneity to be mixed and freeze-dried. Algal hydrolysate for HTM experiments were prepared by dissolving 6.6 g of freeze-dried hydrolysate powder in 350 mL Milli-Q

water. Dionex ICS-5000 AAA-Direct Ion Chromatography (IC) instrument (Thermo Fisher Scientific) equipped with the Dionex IonPacTM CS16 column and a guard column was used to evaluate the dissolved phosphate before and after each HTM reaction. Atomic absorption spectrophotometry (AA-87000, Shimadzu) was used to detect calcium. A 27 mL custom designed stainless steel reactor from HIP Company (High Pressure Equipment Co.) was used for HTM reactions. Omega pressure gauge and thermocouple (P/N: TJ36-CAXL-116G-6, Omega Engineering, Inc.) were connected through a taper seal cross (P/N: 10-24AF4, High Pressure Equipment Co.) to the top of the reactor to continuously monitor pressure and temperature during the reaction (Figure S1, Supporting Information). Calcium hydroxide (equal to Ca/PO₄ molar ratio of 1.67 as a theoretical value for HAp precipitation) and 50 mg of commercial hydroxyapatite (reagent grade, Sigma-Aldrich) were added as mineralizer and seeding material, respectively. A Techne SBS-4 fluidized sand bath which equipped with a Techne TC-9D temperature and airflow controller was used as a heating source (Figure S1, Supporting Information). HTM processes were conducted at 280 °C and 2000 psi. This temperature was selected because algae hydrolysate is the product of FH at 280 °C and it can be efficient for heat integration. Different residence times including 5, 15, 30, 45, 60, and 90 min were tested in duplicate in the HTM process. After each run, the reactor was allowed to cool down in a water bucket to room temperature in about 2-3 min and products were centrifuged and filtered (0.22 µm mixed cellulose esters membrane, Merck Millipore Ltd.) to collect precipitates for further characterization. Precipitates dried at 60 °C were analyzed by X-ray diffraction (XRD, MiniFlex II Desktop X-ray Diffractometer, Rigaku Corp.) in the range of 10 to 80° $(2\theta/\theta)$ with the scan speed of 2 deg/min at 30 kV and 15 mA followed by the peak analysis using Rigaku PDXL software (version 1.8.0.3). TGA was used for studying the thermal stability of the precipitated mineral in temperature range of 25-1200 °C in nitrogen atmosphere with the flow rate of 30 mL/min in an alumina (Al₂O₃) sample holder. This included a steady temperature ramp of 10 °C/min until 500 °C, with a stepwise function (1 °C/min) at 90-110 °C, followed by 3 h hold at 500 °C. The heating continued the rate of 5 °C/min until reached 1200 °C and hold for 1 h. The functional groups were evaluated by fourier Transform infrared spectroscopy (FTIR) (IR Prestige-21, Shimadzu) with 256 scans over a range of 400-4000 cm and a resolution of 4 cm⁻¹. Morphology of the precipitated minerals in addition to elemental characterization and mapping was performed by scanning electron microscopy (SEM, JEOL JSM-6060LV, Tokyo, Japan) featured with energy-dispersive X-ray spectroscopy (EDS, Thermo Electron NORAN System SIX). Aqueous phase was analyzed for phosphate and calcium as well as nitrogen and carbon content after each run. Figure 1 shows the overall process including analyses methods.

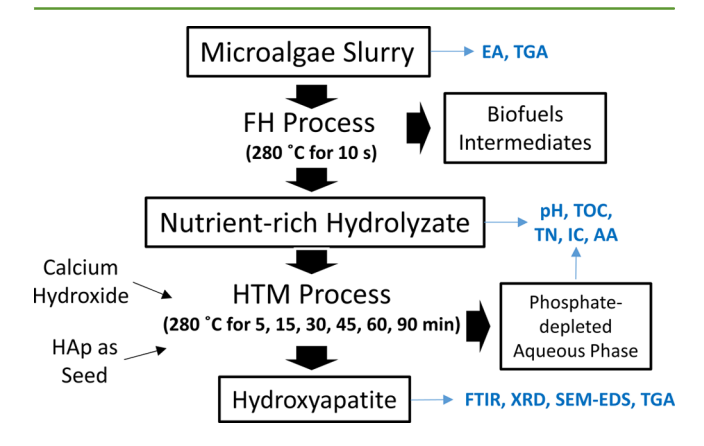


Figure 1. Schematic diagram of the overall process (black) and products analyses (blue). Note: All analyses were performed in duplicate unless otherwise stated.

■ RESULTS AND DISCUSSION

Ultimate and proximate analysis of the Scenedesmus sp. microalgae harvested for this study is shown in Table 1.

Table 1. Scenedesmus sp. Ultimate and Proximate Analysis; Ultimate Analysis is Provided on an Ash Free Dry Weight Percent

ultimate analysis	wt % (±standard deviation)	proximate analysis	wt % (±standard deviation)
carbon	49.1 ± 0.3	moisture	6.5 ± 0.3
nitrogen	7.3 ± 0.1	ash	13.2 ± 0.1
hydrogen	7.1 ± 0.1	volatiles	68.1 ± 0.1
aoxygen	36.5	fixed carbon	12.2 ± 0.2

^aOxygen was calculated based on the difference (C + H + N + O =

The reconstituted hydrolysate was analyzed for TOC, TN, phosphate, and calcium contents prior to HTM process. The results came up as 6670.0 ± 8.5 , 1295.0 ± 9.9 , 665.1 ± 3.9 , and 34.4 ± 1.1 mg/L, respectively. These data were used to evaluate the stoichiometric amount of mineralizer (calcium hydroxide) required to prepare Ca/PO₄ equal to 1.67 for HAp precipitation reaction. The high concentration of nitrogen is due to proteinaceous compounds such as peptides and amino acids extracted after FH process from algal biomass.⁶ The effect of amino acids and soluble peptides on the mineralization process of HAp is an important topic that is still under debate.³⁰ However, at the HTM reaction conditions, they will all decompose to ammonia and other degradation products.8 Another important factor in the HAp synthesis from algal biomass is the usage of seeding material. It has been reported that seeding material could promote crystallization and the amount does not have a considerable effect on the crystal growth rate. 31,32 Similarly, Brown and Fulmer's research revealed that seeding with HAp accelerated the initial reaction for HAp formation.²⁹ The use of HAp seeds will result in stoichiometric crystalline HAp without the formation of precursor phases.³³ Study conducted by Kubota et al. showed that the seed loading is a critical factor in controlling the crystal size distribution (CSD) in the crystallization of potassium alum. They also emphasized that the high concentration of seeds will eliminate the secondary nucleation phenomena in the cooling process.³⁴ In addition, our preliminary results have also explained the crucial role of the seeding material for hydroxyapatite crystallization.²⁶ Therefore, equal amount of commercial HAp (50 mg) was used for each experiment as seeding material.

Same analysis were done on the phosphate-depleted aqueous phase after each reaction to evaluate the nutrient removal kinetics. The following equation (eq 1) has been applied for each component's removal as weight percentage of its total concentration.

removal of component i (wt%)

$$= [(C_{i,in} - C_{i,out})/C_{i,in}] \times 100$$
 (1)

where $C_{i, in}$ is the concentration of component i in the hydrolysate before HTM reactions, and $C_{i, out}$ is the concentration of component i after HTM reactions. The results revealed that 97.1 \pm 0.4 wt % of phosphate and 93.7 \pm 0.3 wt % of calcium removed in the first 5 min of HTM process in forms of calcium phosphate precipitates. Both the rate and

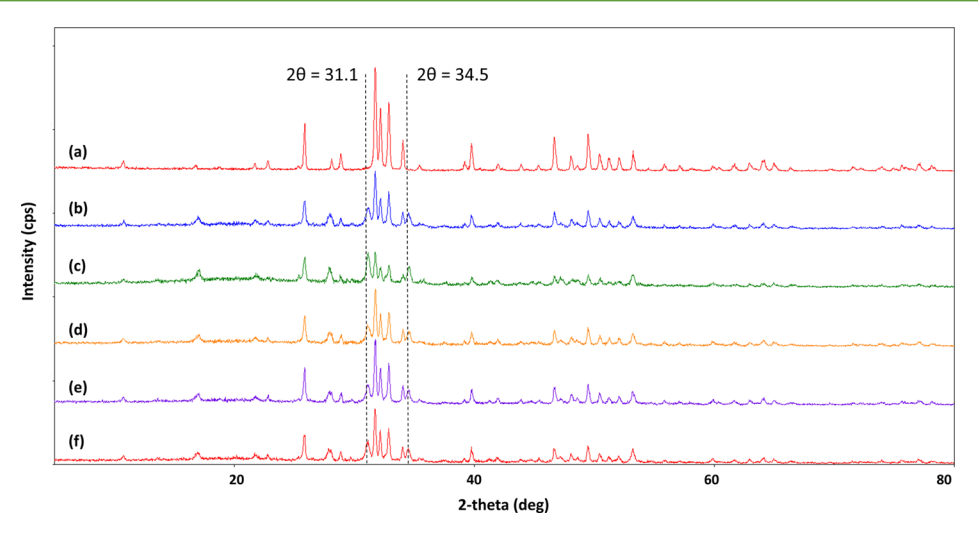


Figure 2. X-ray diffraction patterns for (a) commercial HAp, and HTM experiments conducted at 280 °C and reaction times of (b) 90 min, (c) 60 min, (d) 45 min, (e) 30 min, (f) 15 min. Peaks that are marked with dashed-line at $2\theta = 31.1$ and 34.5 identified as WH.

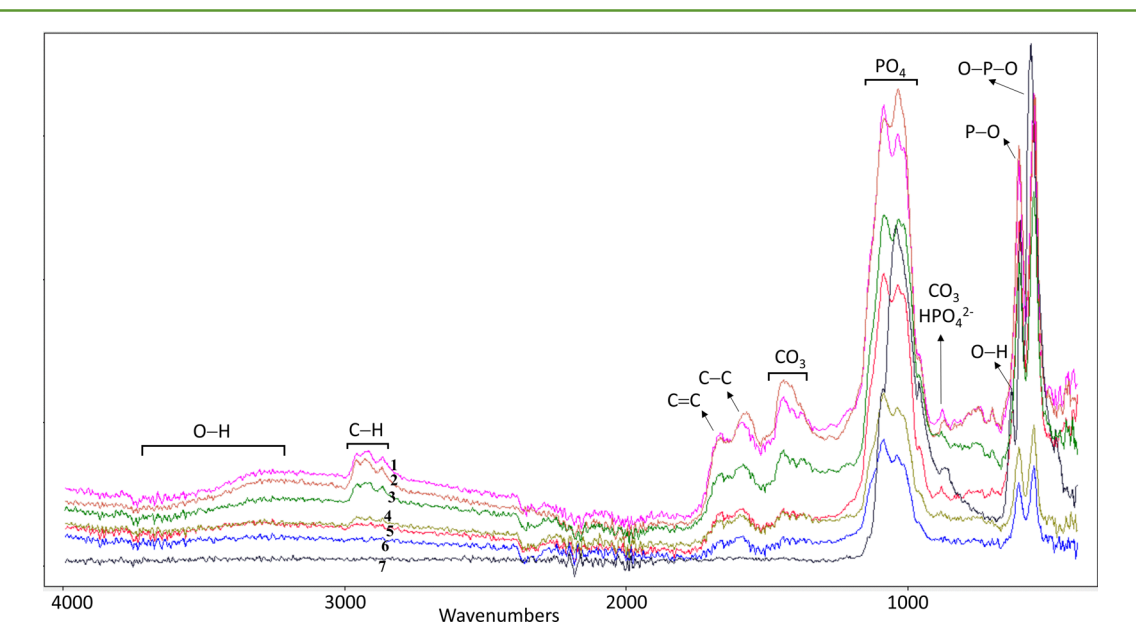


Figure 3. FTIR spectrum of precipitates recovered after 5 min (#5), 15 min (#6), 30 min (#1), 45 min (#4), 60 min (#2), and 90 min (#3) of residence time in the HTM process and their comparison with the commercial HAp (#7).

the extent of recovery in this study is much higher compared to similar studies. For instance, Yu et al. reached 74 or 92 wt % of phosphate removal after 2 or 4 h of reaction time in the form of HAp, respectively. Results revealed by Chen et al. showed phosphate removal of 91.3 wt % after 24 h reaction as HAp. This is also confirmed by a review study performed by Shadat-Shojai et al. in which the majority of HAp formations occurred in 3–120 h of residence time excluding the production pathways. 1

Carbon and nitrogen content of the aqueous phase have also reduced by 10.4 ± 0.6 wt % and 4.6 ± 1.3 wt % in the shortest (5 min) HTM reaction, respectively. Carbon reduction might be due to the decarboxylation or decarbonylation of organic carbon under hydrothermal conditions,³⁷ while degradation of proteinaceous compounds to ammonia might be the reason for nitrogen content reduction.³⁸ This could be the reason for the pH increase of the reaction media from 5.6 before HTM process to approximately 7.2 after the reaction. The precipitates recovered after each run were fully characterized. The

precipitated minerals were compared with commercial HAp (as a reference) during XRD analysis (Figure 2) as well as the international center for diffraction data (ICDD) data bank in terms of peaks intensity and position via the Rigaku PDXL software. Precipitates were assigned as carbonated HAp (JCPDS# 01-076-0694) while the presence of WH (JCPDS# 01-070-2064) has been also observed as the secondry phase. Peaks related to WH have been marked with dashed-line (Figure 2). Mg²⁺ and HPO₄²⁻ ions play a structural role in the WH formation and both are readily available in the algal hydrolysate (eq 2).

$$18Ca^{2+} + 2Mg^{2+} + 14PO_4^{3-} + 2H^+$$

$$\rightarrow Ca_{18}Mg_2(HPO_4)_2(PO_4)_{12}$$
(2)

Mg²⁺ is one of the essential microalgae nutrients due to its role in chlorophyll molecule and algal cell wall while the later anion is the major phosphate species in the slightly acidic pH range (5.6) of the hydrolyzate.³⁹ It has also been reported that the

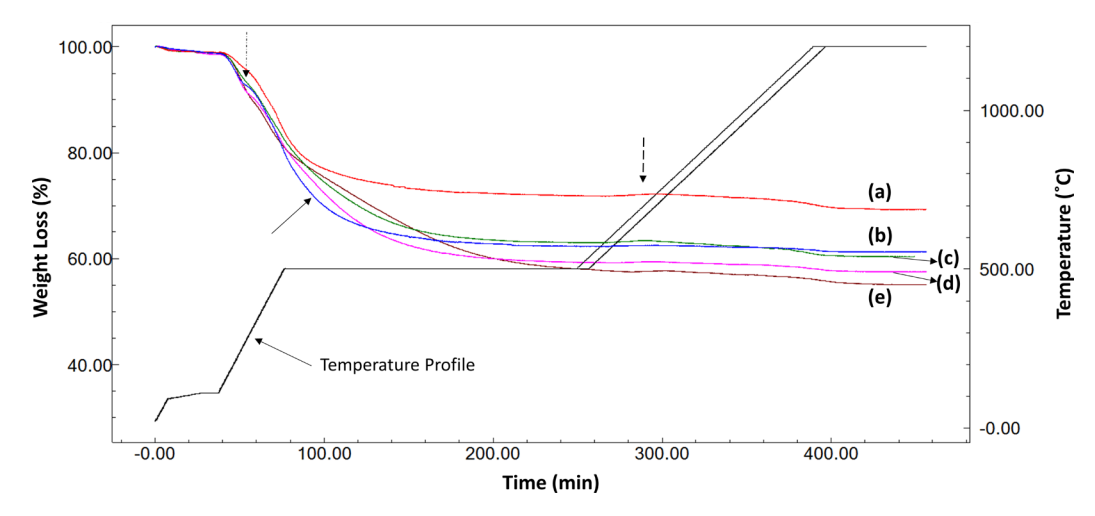


Figure 4. TGA patterns for HTM experiments conducted at 280 °C and reaction times of (a) 5 min, (b) 90 min, (c) 15 min, (d) 45 min, (e) 30 min. Black line indicates the TGA temperature profile.

Table 2. Quantitative Results from the EDS Analysis of Precipitates in Various Retention Times^a

HTM reaction time, min	C, wt %	O, wt %	Mg, wt %	P, wt %	Ca, wt %	Ca/P mol. ratio
15	ND	35.40	0.58	14.75	36.41	1.91
30	5.56	34.60	1.62	14.78	30.49	1.59
45	18.66	31.99	1.02	11.27	25.10	1.72
90	ND	39.07	0.26	16.73	36.24	1.67

"ND: Not detected. The carbon peaks were observed in the EDS pattern; however, the corresponding peak was overlapped by the oxygen peak."

presence of magnesium in the reaction solution impedes the formation of HAp in the favor of WH. 40

Figure 3 shows the FTIR spectra of all the precipitates. The HAp and WH related peaks as well as peaks due to organic carryovers from the carbon-rich microalgae hydrolysate on the precipitates were recognized. Peaks revealed in the range of 2860-2960 cm⁻¹ (C—H stretch), 1668 cm⁻¹ (C—C stretch), 1588 cm⁻¹ (C—C) originated from organic and aromatic compounds carryovers. Peaks at 1087, 1038, 1013 cm⁻¹ $(PO_4-\nu_3)$, 960 cm⁻¹ $(PO_4-\nu_1)$, 564 cm⁻¹ $(PO_4-\nu_4)$, 602 cm⁻¹ (PO $-\nu_4$), 476 cm⁻¹ (PO $_2$ - δ), observed in all precipitates as well as the commercial HAp. However, the sharp small peaks at 634 cm⁻¹ (OH⁻) detected only in commercial HAp. Absence of the (OH-) peak, which is as a result of the water associated with the HAp lattice, confirmed the formation of substituted HAp by XRD analysis. Peaks observed at 1383 cm⁻¹ (CO₃ $-\nu_3$), $1445 \text{ cm}^{-1} (\text{CO}_3^{2-})$ are indication for nonstoichiometric B-type carbonate substitution in the HAp lattice. 41,42 It has been reported that ionic and cationic substitutions have improved the biomedical properties of HAp. 41 Some recent studies have shown that carbonate substitution in HAp structure enhances the biocompatibility characterization and bone regeneration. 43,44 Peaks relevant to the OH group in the lattice are observed in the range of 3500-3600 cm⁻¹. These peaks are a result of water in the HAp lattice and were not observed in the spectrum of TCP (tricalcium phosphate). 45,46 The small sharp peak observed at 880 cm⁻¹ might be a result of either HPO₄²⁻ or CO₃²⁻ in the calcium deficient HAp. 47,48 The intensity of this peak dropped as the reaction time in the HTM process increased and almost disappeared for the precipitates from the 90 min experiment indicating the conversion to the stoichiometric HAp. This has been confirmed with the EDS analysis explained later.

Figure 4 indicates the TGA of samples. As observed, there are similar trends for all precipitated powder including a minor weight loss near 110 °C due to the moisture content and a major weight loss up to 500 °C, which is related to residual organic matter from the carbon-rich algal hydrolysate.²² Powder obtained after 90 min reaction time has relatively, higher weight loss up to 500 °C (solid arrow in Figure 4b). This might be due to higher carbonate in the HAp lattice that has reduced its thermal stability.²² There was also a notable change in the weight loss rate for the same sample as well as the powder related to the 45 min HTM process, which are marked with a dot arrow near 270 °C. This change might correspond to the detachment of adsorbed water followed by the loss of the water in the lattice. 22,49 In all samples, there was weight gain at around 600 °C, which had inverse relation with the residence time of the HTM process. This might be a result of hydroxyl ions uptake into the lattice of hydroxyapatite during the crystallization process. 50 Another weight loss started around 1150 °C for all precipitates, which could have originated from the HAp dihydroxylation. Overall, precipitates from the HTM process after 90 min of reaction time had less than 1.0% weight loss in the range of 500-1200 °C, which is similar to commercial HAp thermal stability. These findings were in agreement with prior results that by increasing the HTM reaction time, precipitates predominately formed HAp rather than WH. This hypothesis was further supported through the elemental composition of the recovered powder using EDS analysis (Table 2). Presence of magnesium and carbon have been observed as they are required for the WH and carbonated HAp formation, respectively. However, the amount of magnesium was the lowest (0.26 wt %) in the minerals recovered after 90 min of reaction time. In addition, Ca/P molar ratio for the precipitated powder matched the ratio of Ca/P = 1.67 in HAp. The small amount of Mg^{2+} might be due

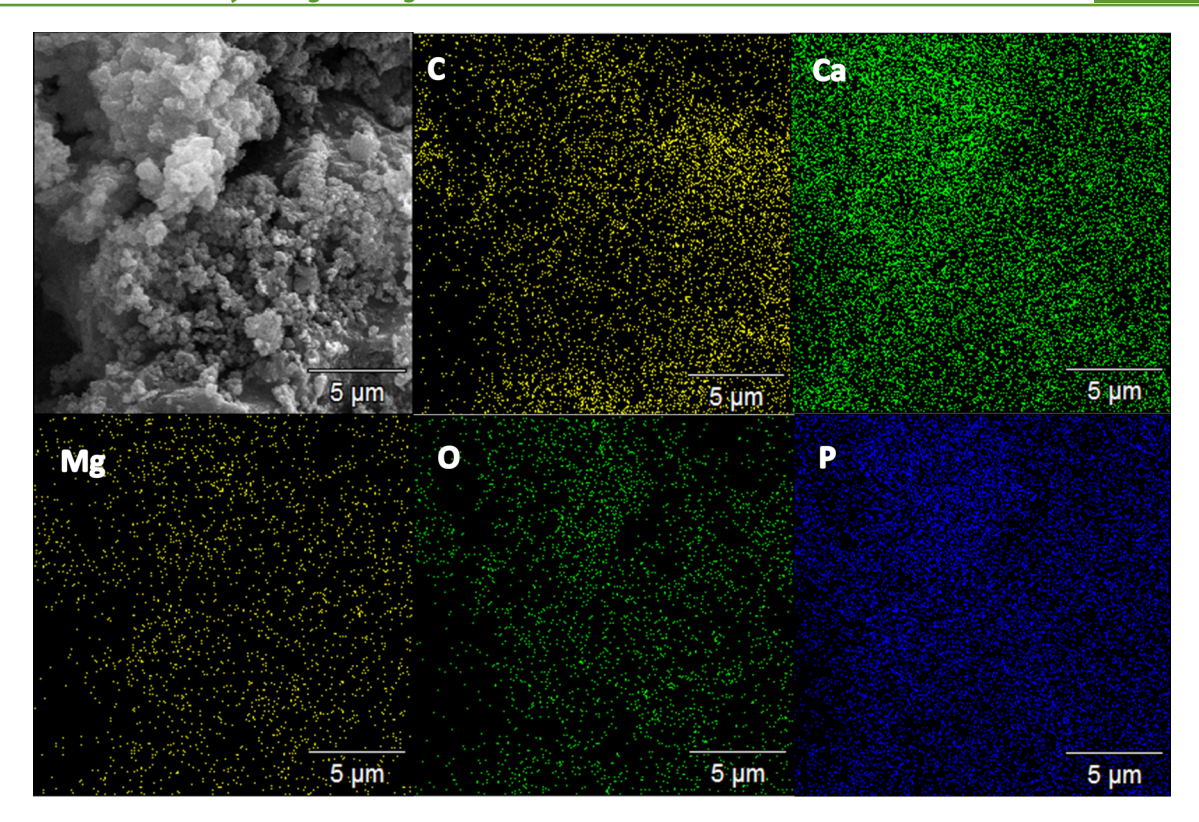


Figure 5. Elemental mapping of carbon, calcium, phosphorus, oxygen, and magnesium of precipitated minerals after 90 min of HTM process.

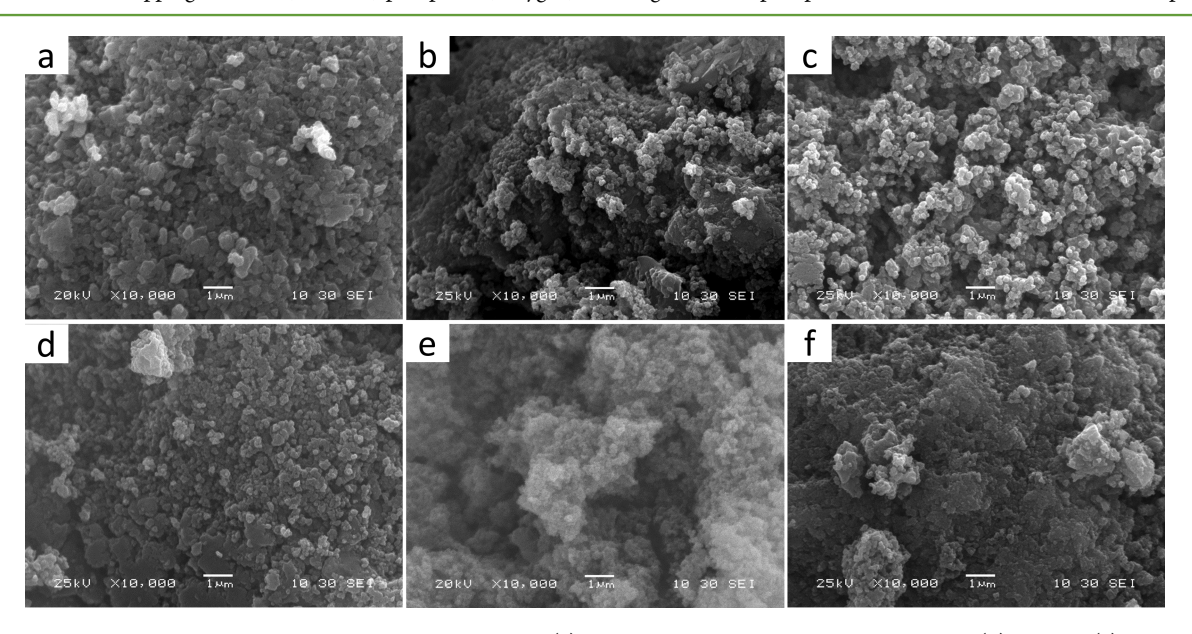


Figure 6. SEM images of commercial HAp used as seeding material (a), and the precipitated material after 15 min (b), 30 min (c), 45 min (d), 60 min (e), and 90 min (f) of HTM process. All images have the same 10,000× magnification.

to the incorporation of this cation in the structure of HAp lattice. Low magnesium content (<1 wt %) could be substituted in HAp without structural changes. This is the case for HAp in human bone as well. Figure 5 demonstrates the two-dimensional elemental mapping of the minerals recovered after 90 min of the HTM process. The results indicate the ubiquitous presence of the carbon, calcium, magnesium, phosphorus, and oxygen elements in the precipitates. The uniform distribution of magnesium in the HAp lattice is in agreement with prior studies. This uniformity also applies to the Ca and P elements of HAp

composition. This would contribute to the good bone osseointegration of HAp particles for biomediacal applications. 52

Morphology of the precipitates recovered after each experiment was analyzed through SEM analysis (Figure 6). As the HTM reaction time increased, small spherical particles of HAp (seeding material) became larger and changed to flat agglomerates. These morphologies are similar to the Palazzo et al. study in which calcium deficient HAp (CDHA) precipitated in the presence of amino acids. ⁵³

Overall, the results from this study showed that phosphate and calcium removal from the algal hydrolyzate mainly occurred in the first 5 min of reaction time. Based on the XRD, FTIR, and EDS analysis, calcium phosphate minerals were discovered to be a mixture of WH and carbonated HAp. However, as the reaction time increased, HAp tended to be the predominant species. This was confirmed by the Ca/P ratio of 1.67 (equal to HAp ratio) for the minerals of experiment performed at 90 min of residence time. These precipitates followed similar thermal behavior as the pure commercial HAp, which was used as a control. In addition, magnesium was detected through EDS analysis to be minimally incorporated through the HAp lattice.

CONCLUSIONS

This work investigates the effect of phosphate removal from the *Scenedesmus* sp. microalgae hydrolysate in the forms of HAp and WH through the integrated FH-HTM process. Majority of phosphate and calcium removal from the hydrolysate occurred in the first 5 min of reaction; however, by tuning the reaction time, calcium phosphate minerals transformed from WH to carbonated HAp with the Ca/P molar ratio of 1.67 after 90 min of residence time. The morphology of particles changed from small spherical in seeding material to larger flat agglomerates. Overall, 80 wt % of phosphorus in the microalgae was recovered in the forms of WH and HAp, which could be used for biomaterials applications.

ASSOCIATED CONTENT

S Supporting Information

The Supporting Information is available free of charge on the ACS Publications website at DOI: 10.1021/acssuschemeng.7b02951.

Schematic diagram of the experimental setup of the HTM reactor (PDF)

AUTHOR INFORMATION

Corresponding Author

*S. Kumar. E-mail: skumar@odu.edu; Tel.: 757-683-3898; Fax: 757-683-5354.

ORCID

Ali Teymouri: 0000-0003-2474-1578

Notes

The authors declare no competing financial interest.

■ ACKNOWLEDGMENTS

The authors acknowledge the financial supports of this work by National Science Foundation (NSF) through the NSF CAREER Award CBET-1351413 and NSF PFI: AIR TT Grant 1640593 and Dr. Wei Cao at Applied Research Center (Newport News, VA) for the assistance with the XRD and SEM-EDS analysis.

■ REFERENCES

- (1) Su, Y.; Song, K.; Zhang, P.; Su, Y.; Cheng, J.; Chen, X. Progress of microalgae biofuel's commercialization. *Renewable Sustainable Energy Rev.* **2017**, *74*, 402–411.
- (2) Quinn, J. C.; Davis, R. The potentials and challenges of algae based biofuels: a review of the techno-economic, life cycle, and resource assessment modeling. *Bioresour. Technol.* **2015**, *184*, 444–52.
- (3) Shurtz, B. K.; Wood, B.; Quinn, J. C. Nutrient resource requirements for large-scale microalgae biofuel production: Multi-

- pathway evaluation. Sustainable Energy Technologies and Assessments 2017, 19, 51-58.
- (4) Jasinski, S. M. Minerals Yearbook, Phosphate Rock; United States Geological Survey, 2015.
- (5) Zhang, T. Y.; Hu, H. Y.; Wu, Y. H.; Zhuang, L. L.; Xu, X. Q.; Wang, X. X.; Dao, G. H. Promising solutions to solve the bottlenecks in the large-scale cultivation of microalgae for biomass/bioenergy production. *Renewable Sustainable Energy Rev.* **2016**, *60*, 1602–1614.
- (6) Garcia-Moscoso, J. L.; Obeid, W.; Kumar, S.; Hatcher, P. G. Flash hydrolysis of microalgae (Scenedesmus sp.) for protein extraction and production of biofuels intermediates. *J. Supercrit. Fluids* **2013**, *82*, 183–190
- (7) Kumar, S.; Hablot, E.; Moscoso, J. L. G.; Obeid, W.; Hatcher, P. G.; DuQuette, B. M.; Graiver, D.; Narayan, R.; Balan, V. Polyurethanes preparation using proteins obtained from microalgae. *J. Mater. Sci.* **2014**, *49* (22), 7824–7833.
- (8) Garcia-Moscoso, J. L.; Teymouri, A.; Kumar, S. Kinetics of Peptides and Arginine Production from Microalgae (Scenedesmus sp.) by Flash Hydrolysis. *Ind. Eng. Chem. Res.* **2015**, *54* (7), 2048–2058.
- (9) Teymouri, A.; Kumar, S.; Barbera, E.; Sforza, E.; Bertucco, A.; Morosinotto, T. Integration of biofuels intermediates production and nutrients recycling in the processing of a marine algae. *AIChE J.* **2017**, 63 (5), 1494–1502.
- (10) Barbera, E.; Teymouri, A.; Bertucco, A.; Stuart, B. J.; Kumar, S. Recycling Minerals in Microalgae Cultivation through a Combined Flash Hydrolysis—Precipitation Process. *ACS Sustainable Chem. Eng.* **2017**, *5* (1), 929—935.
- (11) Barbera, E.; Sforza, E.; Kumar, S.; Morosinotto, T.; Bertucco, A. Cultivation of Scenedesmus obliquus in liquid hydrolysate from flash hydrolysis for nutrient recycling. *Bioresour. Technol.* **2016**, 207, 59–66.
- (12) Talbot, C.; Garcia-Moscoso, J.; Drake, H.; Stuart, B. J.; Kumar, S. Cultivation of microalgae using flash hydrolysis nutrient recycle. *Algal Res.* **2016**, *18*, 191–197.
- (13) Sasai, R.; Matsumoto, Y.; Itakura, T. Continuous-flow detoxification treatment of boron-containing wastewater under hydrothermal conditions. *J. Ceram. Soc. Jpn.* **2011**, *119* (1388), 277–281.
- (14) Itakura, T.; Imaizumi, H.; Sasai, R.; Itoh, H. Phosphorus mineralization for resource recovery from wastewater using hydrothermal treatment. *J. Ceram. Soc. Jpn.* **2009**, *117* (1363), 316–319.
- (15) Sopyan, I.; Mel, M.; Ramesh, S.; Khalid, K. A. Porous hydroxyapatite for artificial bone applications. *Sci. Technol. Adv. Mater.* **2007**, 8 (1–2), 116–123.
- (16) Mori, K.; Hara, T.; Mizugaki, T.; Ebitani, K.; Kaneda, K. Hydroxyapatite-Bound Cationic Ruthenium Complexes as Novel Heterogeneous Lewis Acid Catalysts for Diels—Alder and Aldol Reactions. J. Am. Chem. Soc. 2003, 125 (38), 11460—11461.
- (17) Lovón-Quintana, J. J.; Rodriguez-Guerrero, J. K.; Valença, P. G. Carbonate hydroxyapatite as a catalyst for ethanol conversion to hydrocarbon fuels. *Appl. Catal., A* **2017**, *542*, 136–145.
- (18) Haider, A.; Haider, S.; Han, S. S.; Kang, I.-K. Recent advances in the synthesis, functionalization and biomedical applications of hydroxyapatite: a review. *RSC Adv.* **2017**, *7* (13), 7442–7458.
- (19) Jokić, B.; Mitrić, M.; Radmilović, V.; Drmanić, S.; Petrović, R.; Janaćković, D. Synthesis and characterization of monetite and hydroxyapatite whiskers obtained by a hydrothermal method. *Ceram. Int.* **2011**, 37 (1), 167–173.
- (20) Qi, M.-L.; He, K.; Huang, Z.-N.; Shahbazian-Yassar, R.; Xiao, G.-Y.; Lu, Y.-P.; Shokuhfar, T. Hydroxyapatite Fibers: A Review of Synthesis Methods. *JOM* **2017**, *69* (8), 1354–1360.
- (21) Sadat-Shojai, M.; Khorasani, M.-T.; Dinpanah-Khoshdargi, E.; Jamshidi, A. Synthesis methods for nanosized hydroxyapatite with diverse structures. *Acta Biomater.* **2013**, *9* (8), 7591–7621.
- (22) Felício-Fernandes, G.; Laranjeira, M. C. M. Calcium phosphate biomaterials from marine algae. Hydrothermal synthesis and characterisation. *Quim. Nova* **2000**, 23, 441–446.
- (23) Jang, H. L.; Jin, K.; Lee, J.; Kim, Y.; Nahm, S. H.; Hong, K. S.; Nam, K. T. Revisiting Whitlockite, the Second Most Abundant Biomineral in Bone: Nanocrystal Synthesis in Physiologically Relevant

- Conditions and Biocompatibility Evaluation. ACS Nano 2014, 8 (1), 634-641.
- (24) Jang, H. L.; Zheng, G. B.; Park, J.; Kim, H. D.; Baek, H.-R.; Lee, H. K.; Lee, K.; Han, H. N.; Lee, C.-K.; Hwang, N. S.; Lee, J. H.; Nam, K. T. In Vitro and In Vivo Evaluation of Whitlockite Biocompatibility: Comparative Study with Hydroxyapatite and β -Tricalcium Phosphate. *Adv. Healthcare Mater.* **2016**, 5 (1), 128-136.
- (25) Jang, H. L.; Lee, H. K.; Jin, K.; Ahn, H.-Y.; Lee, H.-E.; Nam, K. T. Phase transformation from hydroxyapatite to the secondary bone mineral, whitlockite. *J. Mater. Chem. B* **2015**, *3* (7), 1342–1349.
- (26) Teymouri, A; Stuart, B., Kumar, S. Kinetics of phosphate precipitation from the nutrients-rich algal hydrolyzate. In *The 253rd ACS National Meeting*, San Francisco, California, 2017.
- (27) TOMSON, M. B.; NANCOLLAS, G. H. Mineralization Kinetics: A Constant Composition Approach. *Science* **1978**, 200 (4345), 1059–1060.
- (28) Liu, C.; Huang, Y.; Shen, W.; Cui, J. Kinetics of hydroxyapatite precipitation at pH 10 to 11. *Biomaterials* **2001**, 22 (4), 301–306.
- (29) Brown, P. W.; Fulmer, M. Kinetics of Hydroxyapatite Formation at Low Temperature. J. Am. Ceram. Soc. 1991, 74 (5), 934–940.
- (30) Wang, H. Hydroxyapatite degradation and biocompatibility. Ph.D. dissertation, The Ohio State University, 2004.
- (31) Jang, H.; Kang, S.-H. Phosphorus removal using cow bone in hydroxyapatite crystallization. *Water Res.* **2002**, *36* (5), 1324–1330.
- (32) Koutsopoulos, S.; Dalas, E. The effect of acidic amino acids on hydroxyapatite crystallization. *J. Cryst. Growth* **2000**, 217 (4), 410–415
- (33) Inskeep, W. P.; Silvertooth, J. C. Kinetics of hydroxyapatite precipitation at pH 7.4 to 8.4. *Geochim. Cosmochim. Acta* **1988**, 52 (7), 1883–1893.
- (34) Kubota, N.; Doki, N.; Yokota, M.; Sato, A. Seeding policy in batch cooling crystallization. *Powder Technol.* **2001**, *121* (1), 31–38.
- (35) Yu, Y.; Wu, R.; Clark, M. Phosphate removal by hydrothermally modified fumed silica and pulverized oyster shell. *J. Colloid Interface Sci.* **2010**, 350 (2), 538–543.
- (36) Chen, X.; Kong, H.; Wu, D.; Wang, X.; Lin, Y. Phosphate removal and recovery through crystallization of hydroxyapatite using Xonotlite as seed crystal. *J. Environ. Sci.* **2009**, *21* (5), 575–580.
- (37) Yu, G.; Zhang, Y. H.; Schideman, L.; Funk, T.; Wang, Z. C. Distributions of carbon and nitrogen in the products from hydrothermal liquefaction of low-lipid microalgae. *Energy Environ. Sci.* **2011**, 4 (11), 4587–4595.
- (38) Toor, S. S.; Rosendahl, L.; Rudolf, A. Hydrothermal liquefaction of biomass: A review of subcritical water technologies. *Energy* **2011**, *36* (5), 2328–2342.
- (39) Esakkimuthu, S.; Krishnamurthy, V.; Govindarajan, R.; Swaminathan, K. Augmentation and starvation of calcium, magnesium, phosphate on lipid production of Scenedesmus obliquus. *Biomass Bioenergy* **2016**, *88*, 126–134.
- (40) Elliott, J. C. Structure and chemistry of the apatites and other calcium orthophosphates; Elsevier, 2013; Vol. 18.
- (41) Roberts, G. W.; Sturm, B. S.; Hamdeh, U.; Stanton, G. E.; Rocha, A.; Kinsella, T. L.; Fortier, M.-O. P.; Sazdar, S.; Detamore, M. S.; Stagg-Williams, S. M. Promoting catalysis and high-value product streams by in situ hydroxyapatite crystallization during hydrothermal liquefaction of microalgae cultivated with reclaimed nutrients. *Green Chem.* 2015, 17 (4), 2560–2569.
- (42) Shu, C.; Yanwei, W.; Hong, L.; Zhengzheng, P.; Kangde, Y. Synthesis of carbonated hydroxyapatite nanofibers by mechanochemical methods. *Ceram. Int.* **2005**, *31* (1), 135–138.
- (43) Shen, D.; Horiuchi, N.; Nozaki, S.; Miyashin, M.; Yamashita, K.; Nagai, A. Synthesis and enhanced bone regeneration of carbonate substituted octacalcium phosphate. *Bio-Med. Mater. Eng.* **2017**, 28 (1), 9–21.
- (44) Szcześ, A.; Hołysz, L.; Chibowski, E. Synthesis of hydroxyapatite for biomedical applications. *Adv. Colloid Interface Sci.*.2017, DOI: 10.1016/j.cis.2017.04.007.

- (45) Destainville, A.; Champion, E.; Bernache-Assollant, D.; Laborde, E. Synthesis, characterization and thermal behavior of apatitic tricalcium phosphate. *Mater. Chem. Phys.* **2003**, *80* (1), 269–277.
- (46) Theophanides, T. M. Infrared Spectroscopy-Materials Science, Engineering and Technology; InTech, 2012.
- (47) Berzina-Cimdina, L.; Borodajenko, N. Research of calcium phosphates using Fourier transform infrared spectroscopy. In *Infrared Spectroscopy Materials Science, Engineering and Technology*; Theophanides, T., Ed.; InTech, 2012.
- (48) Ren, F.; Leng, Y.; Ding, Y.; Wang, K. Hydrothermal growth of biomimetic carbonated apatite nanoparticles with tunable size, morphology and ultrastructure. *CrystEngComm* **2013**, *15* (11), 2137–2146.
- (49) Diallo-Garcia, S.; Laurencin, D.; Krafft, J.-M.; Casale, S.; Smith, M. E.; Lauron-Pernot, H.; Costentin, G. Influence of Magnesium Substitution on the Basic Properties of Hydroxyapatites. *J. Phys. Chem. C* **2011**, *115* (49), 24317–24327.
- (50) Gross, K. A.; Gross, V.; Berndt, C. C. Thermal Analysis of Amorphous Phases in Hydroxyapatite Coatings. *J. Am. Ceram. Soc.* **1998**, *81* (1), 106–112.
- (51) Fadeev, I. V.; Shvorneva, L. I.; Barinov, S. M.; Orlovskii, V. P. Synthesis and Structure of Magnesium-Substituted Hydroxyapatite. *Inorg. Mater.* **2003**, 39 (9), 947–950.
- (52) Wei, Q.; Li, S.; Han, C.; Li, W.; Cheng, L.; Hao, L.; Shi, Y. Selective laser melting of stainless-steel/nano-hydroxyapatite composites for medical applications: Microstructure, element distribution, crack and mechanical properties. *J. Mater. Process. Technol.* **2015**, 222, 444–453.
- (53) Palazzo, B.; Walsh, D.; Iafisco, M.; Foresti, E.; Bertinetti, L.; Martra, G.; Bianchi, C. L.; Cappelletti, G.; Roveri, N. Amino acid synergetic effect on structure, morphology and surface properties of biomimetic apatite nanocrystals. *Acta Biomater.* **2009**, *5* (4), 1241–1252.